10th ANKARA INTERNATIONAL AEROSPACE CONFERENCE **AIAC-2019-120**
18-20 September 2019 - METU, Ankara TURKEY

COMPUTATIONAL MODELING OF REAL GAS FLOWS OVER SHARP-CONE-FLARE AND BLUNT CONE GEOMETRIES

Cihangir Celal Palacı[1] and Ahmet Selim Durna[2]
Samsun University
Samsun, Turkey

ABSTRACT

In the present study, real gas flow fields over sharp-cone-flare and blunt cone geometries, which are chemically reacting, are modeled by using a commercial Computational Fluid Dynamics (CFD) software. For CFD validation with experimental data, real gas hypersonic flow fields are simulated and compared with experimental data specifically designed to recreate conditions found by hypersonic vehicles. Results of numerical simulations validated with the results available in the literature. Good correlation is observed between the results from the commercial code with the experimental data with small discrepancies due to the lack of vibrational non-equilibrium.

INTRODUCTION

It is essential to be able to predict the aerodynamic properties of a vehicle with reasonable accuracy, to design realistic aerodynamic vehicles to fly in the hypersonic regime. It would be an unproductive effort to try to predict the flow field over a complex body without the ability to predict over a simple generic one [Kussoy and Horstman, 1989]. In this context, two geometries convenient to simulate in the real gas flow field are chosen.

In the case of reentry flight condition, a blunt-nosed vehicle travels through the atmosphere at hypersonic velocities, and the flow is typically characterized by the presence of a strong bow shock. On the other hand, the vehicles which have a conical-shaped nose are often used practically at hypersonic velocities.

For the flow simulation of the vehicles that moving at the speeds above the speed of sound, especially at hypersonic speeds, the ideal gas law does not work, if the species contained in the studied atmosphere are chemically reacting (e.g. dissociation, atomization) and therefore the chemical reactions occurring must also be modeled [Anderson, 2006].

Various studies can be seen related to computational modeling of real gas flow fields. A parametric study of a hypersonic inlet by validating turbulence models and non-equilibrium flows is performed. Turbulence models' case is performed over a cone-ogive geometry and good correlation is found. Non-equilibrium flow case is performed over a blunt cone geometry with some discrepancies due to lack of vibrational non-equilibrium [Oliden, 2013]. In a study [Sockalingam and Tabiei, 2016], a chemically reacting hypersonic flow for an axisymmetric

[1] Undergraduate Student in Aerospace Engineering Department, Email: cihangircelalpalaci@gmail.com
[2] Assistant Professor in Aerospace Engineering Department, Email: ahmetselim.durna@samsun.edu.tr

vehicle at zero-degree angle of attack is simulated by using a commercial CFD software in which different diffusion models have been applied into, and a good correlation is observed. Another CFD study [Savino and Paterna, 2005] is performed by simulating a flow-field around a blunt cone in hypersonic flow with a close agreement with the experimental data although some discrepancies. Validation study of numerical simulation of supersonic gas flows with thermochemical non-equilibrium by using ANSYS FLUENT with an additional user-defined open-code module is produced. The study demonstrated that the software package can be used for simulating flows with thermochemical non-equilibrium. [Shoev *et al.*, 2016]

In this study, simulated flow field on a sharp and blunt cone with flare are compared with experimental data at Mach 7 [Wadhams *et al.*, 2008] and above Mach 10 [Holden *et al.*, 1997], respectively. After the validation study, three different case studies are performed such that air is used as the fluid, air is modeled as a mixture with the species it contains, and the mixture with the reactions expected to occur. Likewise, these are expected that the effects of vibrational and chemical non-equilibrium for the flow field around the geometries.

METHOD

Geometry

Sharp-cone-flare Model:

The first test body is a sharp-cone-flare with flare, as shown in Figure 1. The model is 1.713 m long, with a 0.275 m diameter at zero angle of attack. The attached flare has a half-angle of 37 degrees. More detail for the test body can be found in [Wadhams *et al.*, 2008].

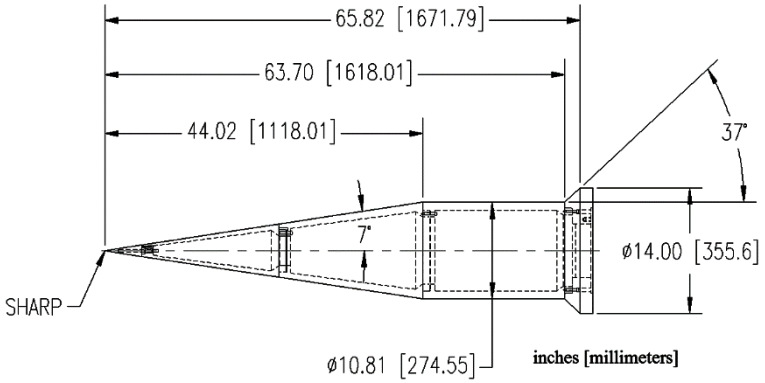

Figure 1: Sharp-cone-flare model in inches and [millimeters] [Wadhams *et al.*, 2008]

Blunt Cone Model:

The second test body is a blunt cone with a flare as shown with its sizes in meters in Figure 2. The non-equilibrium phenomena can be examined as the flow expands around the nose, relaxes along the 15-degree cone, and recompresses over the flare. These sizes are suitable to allow time for the flow to vibrationally and chemically relaxing along the cone. Only Runs 59 and 63 are chosen for this validation case. More detail for the test body can be found in [Holden *et al.*, 1997].

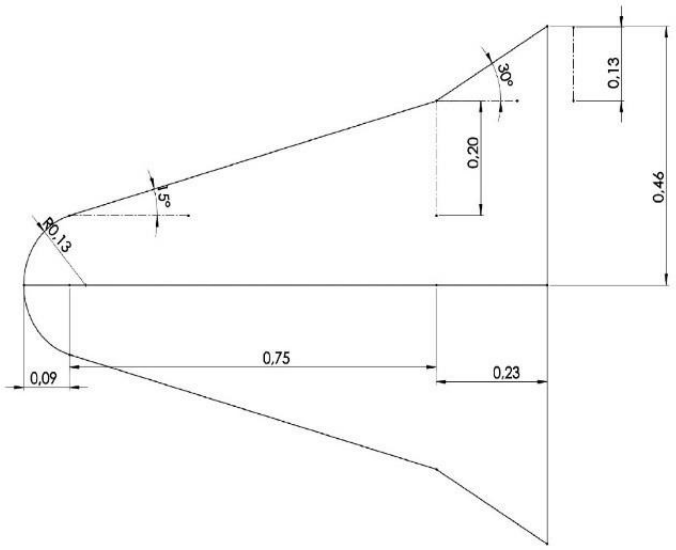

Figure 2: Blunt cone model

Computational Domain

Both computational domains are composed of completely quadrilateral cells. Structured grid is preferred due to its better convergence and higher resolution advantages over unstructured grid. The cell distributions are intensified near the geometry surface where the shocks and pressure differences are expected by the method of inflation as seen in Figure 3 and 4. The grid has a $y^+ \approx 1$, in order to capture the boundary layer correctly. Axisymmetric grids are created with axes defined at the radial centers of the test bodies. This allowed reducing the run time of the simulation while capturing three-dimensional relieving effects.

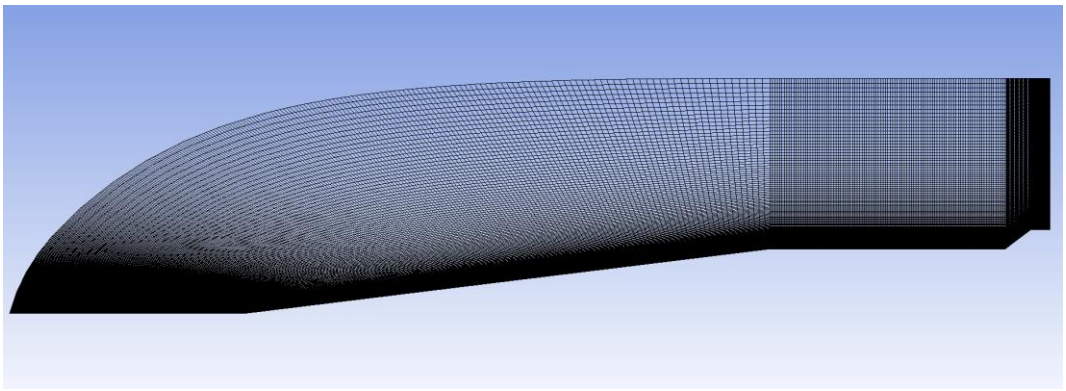

Figure 3: Computational domain for sharp-cone-flare model

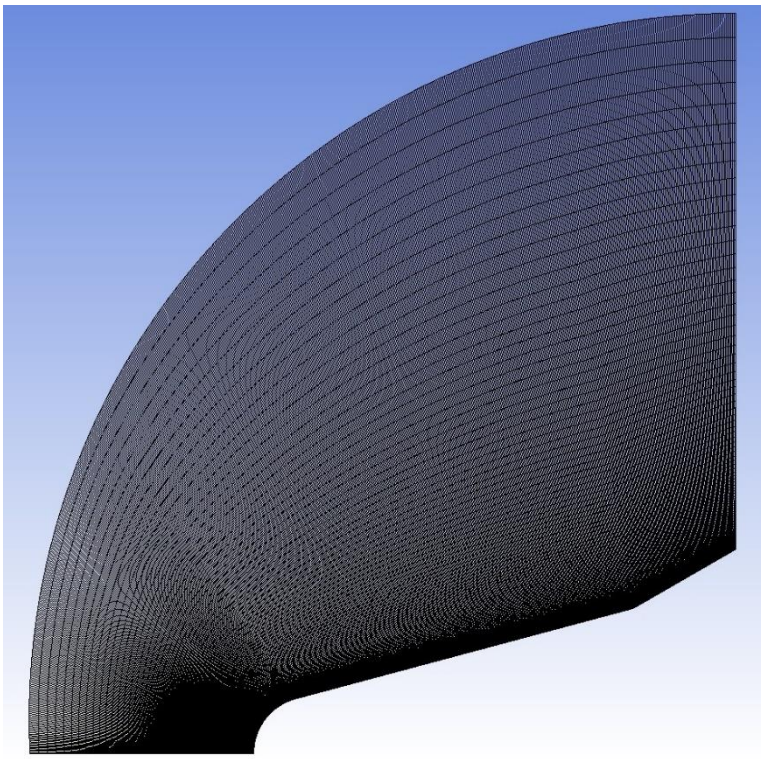

Figure 4: Computational domain for blunt cone model

The mesh is generated in 3 different levels (coarse, medium, fine) and mesh independence study is performed. The number of cells in the tangential direction to the body and the number of cells in the normal direction (i x j), and the total number of cells of the grids can be found in Table 1 and 2. In the study, it is found that the solution is not dependent on the total number of cells, hence it is a mesh independent solution. Medium level grids are preferred for all solutions.

Table 1: Mesh independence study for sharp-cone-flare model

Grid	i x j	Number of Cells
Coarse	340x100	68000
Medium	680x200	136000
Fine	1360x400	272000

Table 2: Mesh independence study for blunt cone model

Grid	i x j	Number of Cells
Coarse	351 x 84	29484
Medium	968 x167	116566
Fine	1396 x 334	466264

Solver Settings

General:

A commercial finite-volume based Navier-Stokes solver, ANSYS FLUENT, is used in the study. In general settings, density-based solvers are chosen. As the solution is assumed to proceed in time until a steady-state solution is reached and the flow properties are independent of the exact time, steady solver is chosen. Axisymmetric solver is chosen due to the axisymmetric modeled geometry.

Models:

The energy equation is enabled to combine the velocity with the static temperature for compressible flow in all cases and species transport is enabled in the cases where the mixture model is used as the fluid.

The species transport is modeled for their respective fluids in each case where mixtures are used as fluid. The type of reaction is set to volumetric, which indicates that the reactions occur in the bulk phase of the flow. Laminar finite-rate is selected for reaction model which computes only the Arrhenius rate.

a) Sharp-cone-flare Model:

The k-kl-ω transition model is used to predict boundary layer development and calculate transition layer. This model can be used to effectively address the transition of the boundary layer from a laminar to a turbulent regime. Turbulence intensity of 1% and turbulence viscosity ratio of 1 used for all simulations.

b) Blunt Cone Model:

In the experimental data**,** it is noted that the flow is laminar throughout the test body and boundary layer separation at the flare is observed. Measurements of pressure and heat transfer from the experiment indicate a small separation region at the cone-flare joint. In this region, flow is known to be laminar, due to the decreasing heat transfer. [Holden *et al.*, 1997]. Therefore, the laminar viscous model is chosen.

Materials:

The ideal gas law is considered a proper thermodynamic relation when Inequality 1 or Inequality 2 and 3 are satisfied [Anderson, 2003]. P_c and T_c correspond critical pressure and critical temperature of the specific gas, respectively. These values are 3,771,432 Pa and 132.65 K [Keunen and Clark, 1917], and 3,395,800 Pa and 126.2 K [Span, Roland, *et al.*, 2000] for air and molecular nitrogen, respectively.

$$\frac{P}{P_C} \ll 1 \tag{1}$$

$$\frac{P}{P_C} < 1 \tag{2}$$

$$\frac{T}{T_C} > 2 \tag{3}$$

For the validation of using the ideal gas model in the simulation, valid assumptions are made to assume those the fluid of Run 59 is pure molecular nitrogen and the fluid of Run 63 is pure air. Therefore, density is calculated using the ideal gas law, for each case modeled.

For the cases where air is used as fluid, the specific heat, thermal conductivity, and dynamic viscosity are calculated using piecewise functions to define these physical properties as a function of temperature. Therefore, these parameters are classified as thermally perfect gas. For the calculation of the specific heat, piecewise-polynomial function is used by defining the coefficients specified by [McBride *et al.*, 1993]. For the calculation of the thermal conductivity and dynamic viscosity, piecewise-linear function is used by defining the coefficients specified by [Kadoya *et al.*, 1985].

For the cases where mixture is used as fluid, since a multicomponent flow modeled which includes more than one chemical species, thermal conductivity and dynamic viscosity are calculated using ideal-gas-mixing-law which is defined as a composition-dependent parameter and correctly couples with the ideal gas law. The specific heat is calculated by using mixing-law. Mass diffusivity is calculated with kinetic theory to calculate macroscopic properties of the mixture depending on its molecular composition.

For the species contained in the mixture, the specific heats of each species are calculated using piecewise-polynomial functions. The function coefficients are specified from [McBride *et al.*, 1993]. Thermal conductivities and dynamic viscosities of each species are calculated using

kinetic theory. To use kinetic theory for the properties of the mixture material, Lennard Jones parameters for each of the constituent species are defined.

For the test bodies for each case, the material types for solid are set to aluminum. Default values are used.

a) Sharp-cone-flare Model:

For the validation of this case with experimental data, air is used as fluid with same settings as mentioned in the previous section. A mixture is created for the reaction case. The materials settings used are selected to be similar to Run 63 which will be found in the next section.

b) Blunt Cone Model:

Runs 59 and 63 are similar test conditions, but with nitrogen and air as the prominent fluids, respectively. For both runs, the stoichiometric and rate exponents for each species of each reaction is 1. Standard state enthalpy, standard state entropy, and the reference temperature for each species are automatically entered by built-in database of the software, where the pre-exponential factor, the temperature exponent, activation energy, and the net effect of third bodies of the reaction are defined manually from [Park and Seung-Ho, 1995].

The Park model which is used for the simulation is a two-temperature model that provides accurate results due to it modeling of translational and vibrational energy modes. The software's default solver only allows for the temperature solved from the energy equation to be used for the reaction rates. Also, the software does not have a built-in vibrational non-equilibrium solver. Since only the static temperature can be defined for the reaction rates, the two-temperature model becomes a one-temperature model of which modeling is limited to vibrational equilibrium and chemical non-equilibrium. Therefore, simulations are run by assuming that the flows in vibrational equilibrium. All reactions are selected to include backward reaction.

Run 59:

A mixture of which species are molecular nitrogen (N_2) and atomic nitrogen (N) is created, where the majority of the fluid is molecular nitrogen. There is no dissociation expected, but Reaction 1 is modeled for validation. At high temperatures or low pressures, real gases deviate insignificantly from ideal gas behavior. [Waals, 1873] M corresponds to the third-body efficiencies for each species.

$$N_2 + M' \leftrightarrow N + N + M' \quad (1)$$

Run 63:

A mixture of which species are molecular nitrogen (N_2), atomic nitrogen (N), molecular oxygen (O_2), atomic oxygen (O), and nitrogen oxide (NO) is created. Ionization process can be neglected, when dissociation and neutral-exchange reactions are modeled for the 5-species air model. [Warnatz *et al.*, 1992] Reactions 2, 3 and 4 are the dissociation reactions, where Reactions 5 and 6 are neutral-exchange reactions.

$$O_2 + M' \leftrightarrow O + O + M' \quad (2)$$

$$N_2 + M'' \leftrightarrow N + N + M'' \quad (3)$$

$$NO + M''' \leftrightarrow N + O + M''' \quad (4)$$

$$N_2 + O \leftrightarrow NO + N \quad (5)$$

$$NO + O \leftrightarrow O_2 + N \quad (6)$$

Boundary Conditions:

Pressure far field is used for freestream conditions are given in each case of the experimental studies. The outlet conditions are identical to the inlet conditions. Also, backflow total temperature is defined for pressure outlet. Backflow is not expected but defined for confirmation. The axes for both grids are the locations of the rotational axes for the geometries.

a) Sharp-cone-flare Model:

Required boundary conditions for reactions are established for the reaction case, which can be found in Table 4.

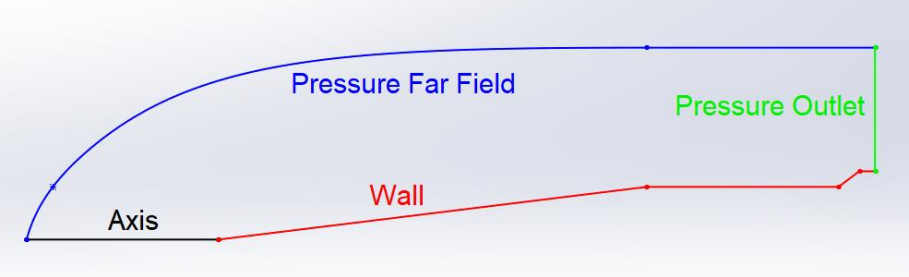

Figure 5: Boundary conditions for sharp-cone-flare model

Table 3: Boundary conditions for sharp-cone-flare model validation case

Inlet (Pressure Far Field)	
Mach Number	7.163
Gauge Pressure (Pa)	4728
Temperature (K)	262
Total Temperature (K)	2615
Laminar Kinetic Energy (m^2/s^2)	809.45
Wall	
Temperature (K)	295
Heat Generation Rate (w/m^3)	0
Wall Motion	Stationary Wall
Shear Condition	No Slip

Table 4: Boundary conditions for sharp-cone-flare model reaction case

Inlet (Pressure Far Field)	
Mach Number	11.11
Gauge Pressure (Pa)	461
Temperature (K)	489.25
Total Temperature (K)	1077
Laminar Kinetic Energy (m^2/s^2)	1202.46
Wall	
Temperature (K)	295
Heat Generation Rate (w/m^3)	0
Wall Motion	Stationary Wall
Shear Condition	No Slip

b) Blunt Cone Model:

Since argon has an insignificant effect at these temperatures, it can be neglected for the used 5-species air model [Aupoix and Cousteix, 1992]. The mole fraction of argon is added onto the mole fraction of molecular nitrogen.

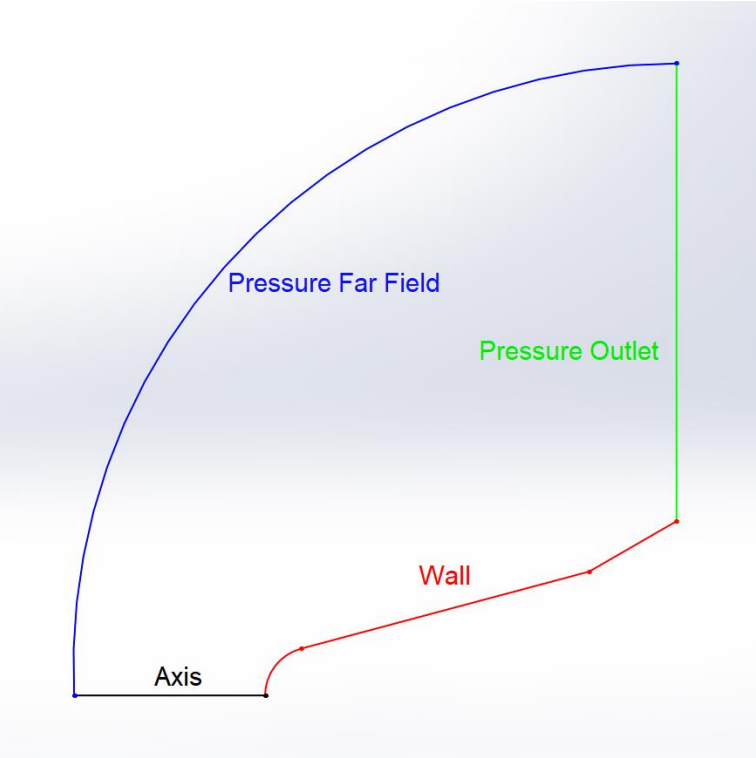

Figure 6: Boundary conditions for blunt cone model

Table 5: Boundary conditions for blunt cone model

Inlet (Pressure Far Field)	**Run 59**	**Run 63**
Mach Number	10.3836	10.3114
Gauge Pressure (Pa)	461	460
Temperature (K)	242.42	226
Total Temperature (K)	4576.5	4020
Gauge Pressure (Pa)	461	460
Temperature (K)	242.42	226
Wall	**Run 59**	**Run 63**
Temperature (K)	295	
Heat Generation Rate (w/m^3)	0	
Wall Motion	Stationary Wall	
Shear Condition	No Slip	

Table 6: Inlet species boundary conditions for blunt cone model

Species Mole Fractions (Inlet)		
Specie	**Run 59**	**Run 63**
N_2	0.9999	0.75744
N	0.0001	0.00489
NO	does not exist	0.00946
O_2	does not exist	0.22821
O	does not exist	0

Solution Methods:

Implicit method is used for formulation for its capability to overcome stiffness in the species transport coupled with Navier-Stokes equations [Warnatz *et al.*, 1992]. The Advection

Upstream Splitting Method (AUSM) is chosen for the flux type to simulate the exact resolution of the shock discontinuities and not to encounter with oscillations at the shocks [ANSYS, 2010]. For the gradient method, green-gauss-cell-based method is used because it is the least fluctuating and the best convergent one. For spatial discretization terms, 1st order upwind scheme method is used until the flow is established, then switched to 2nd order again. This method is followed to overcome the carbuncle phenomenon. Due to carbuncle phenomenon, the calculation is made with the solution steering technique [ANSYS, 2010].

RESULTS

Sharp-cone-flare Model

Validation Case:

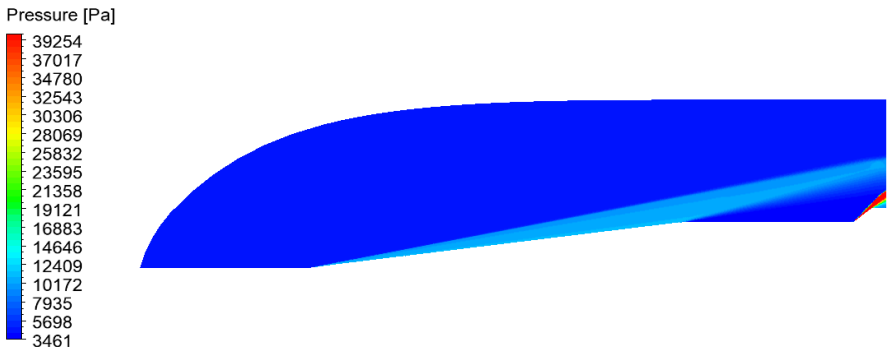

(a)

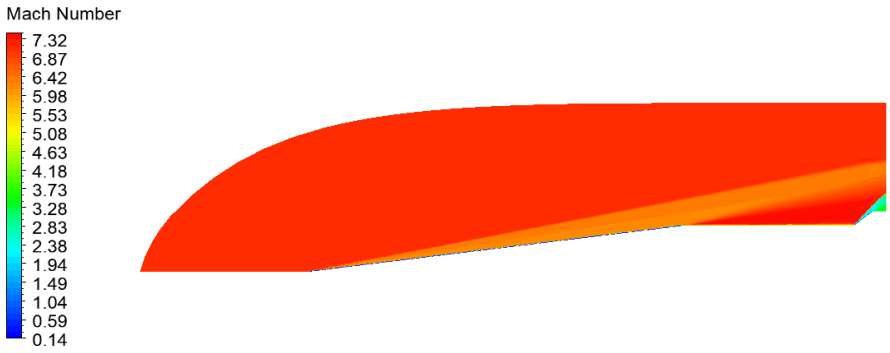

(b)

Figure 7: Pressure (a) and Mach (b) contours for validation case

Pressure and Mach number contours around the sharp-cone-flare test body are found in Figures 7 (a) and (b). A weak oblique shock on the sharp nose and a strong oblique shock on the flare can be seen. It is an expected result causing by the various deflection angles of the inclined surfaces which is a well-known effect for oblique shocks.

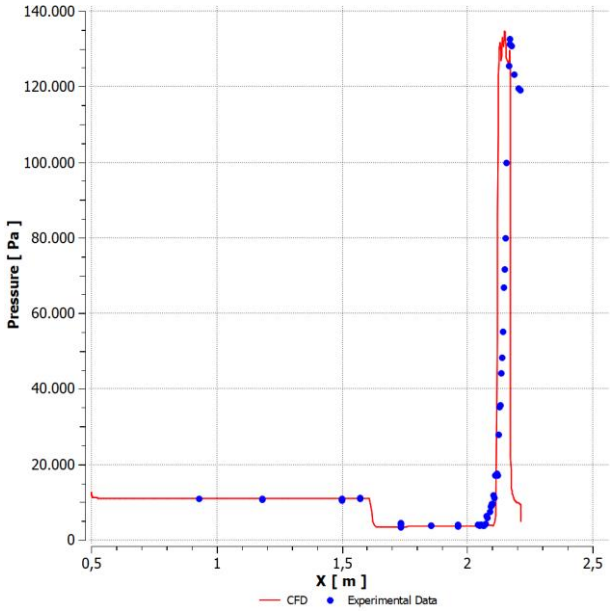

Figure 8: Surface pressure distribution along the body of the sharp-cone-flare

Pressure distribution along the test body surface can be found in Figure 8. A good correlation is found between the experimental data and the simulation modeled for this case, with slight discrepancies near the flare.

Reaction Modeling Case:

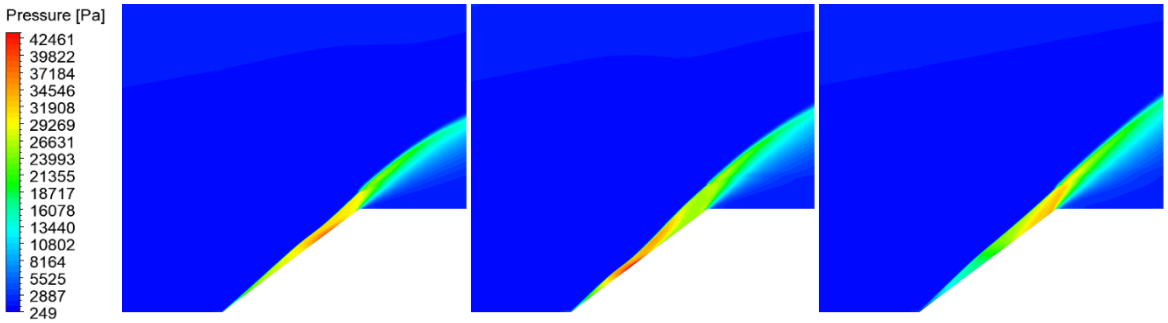

Figure 9: Pressure contours along the flare for reaction case (air, mixture & reaction, respectively)

Refer to Figures 9 (a), (b) and (c) to for pressure distribution on the flare. There are significant differences between the contours. These differences occur by effects of species transport and the energy absorption from reactions. An unexpected pressure distribution observed in mixture case which can be found in Figure 9 (b). This effect may be caused by species-surface interaction or species-boundary layer interaction, which are neglected for this case.

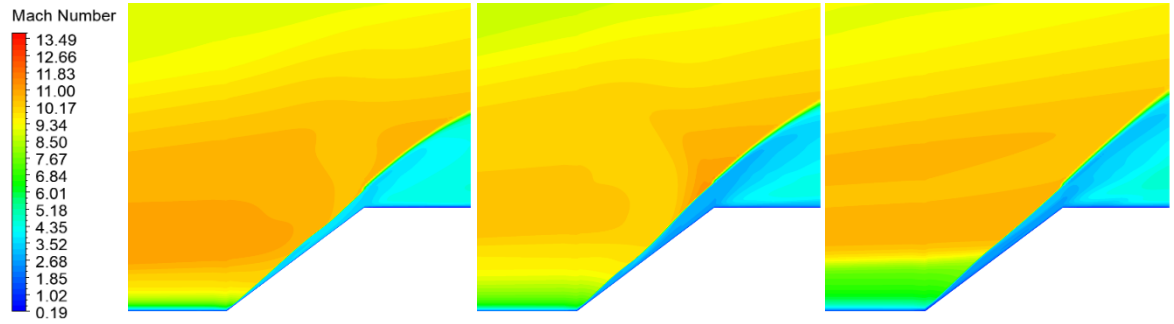

(a) (b) (c)

Figure 10: Pressure contours along the flare for reaction case (air, mixture & reaction, respectively)

Figures 10 (a), (b) and (c) shows the Mach number contours in the flow field on the flare. Oblique shock waves around the flare and the characteristic shock wave-boundary layer interactions in the cylinder–flare junction region can be detected which are the most relevant features of the flow.

Blunt Cone Model

Run 59:

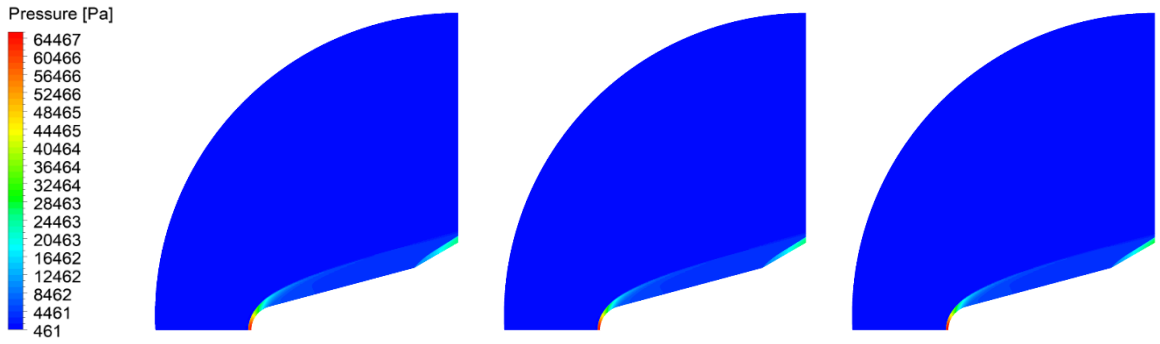

(a) (b) (c)

Figure 11: Pressure contours for Run 59 (air, mixture & reaction, respectively)

Figures 11 (a), (b) and (c) give a general idea of pressure distribution for each separate case. A pressure increase can be seen with a detached bow shock which is formed upstream of the leading edge of the cone. The bow shock wave is weakened progressively as it departs from the stagnation region. There is not a clearly defined oblique shock, but rather a gradual compression at the flare, and a pressure increase observed along the flare.

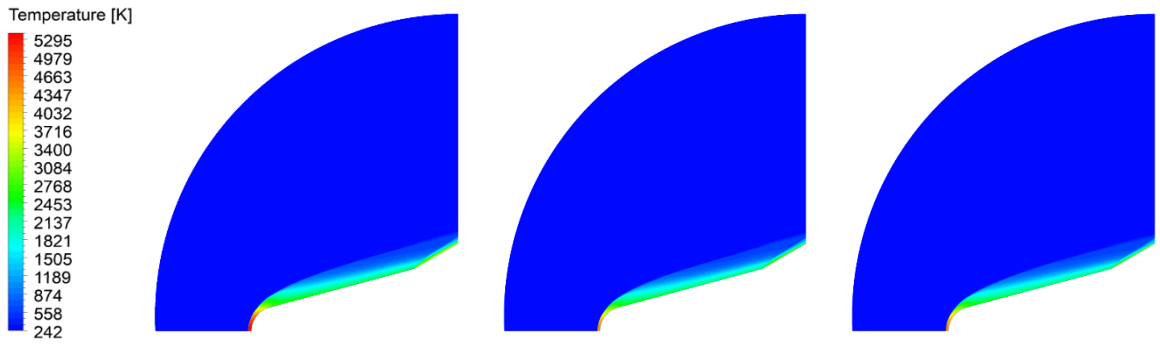

(a) (b) (c)

Figure 12: Temperature contours for Run 59 (air, mixture & reaction, respectively)

Refer to Figures 12 (a), (b) and (c) for temperature distribution around the blunt cone. When the shock wave is followed perpendicularly from the surface of the body, the temperature gradually cools down to freestream temperature. Furthermore, it can be seen in the Figure 12 (a) that the temperature increase in the shock zone for the case where the fluid is air is higher than the other cases.

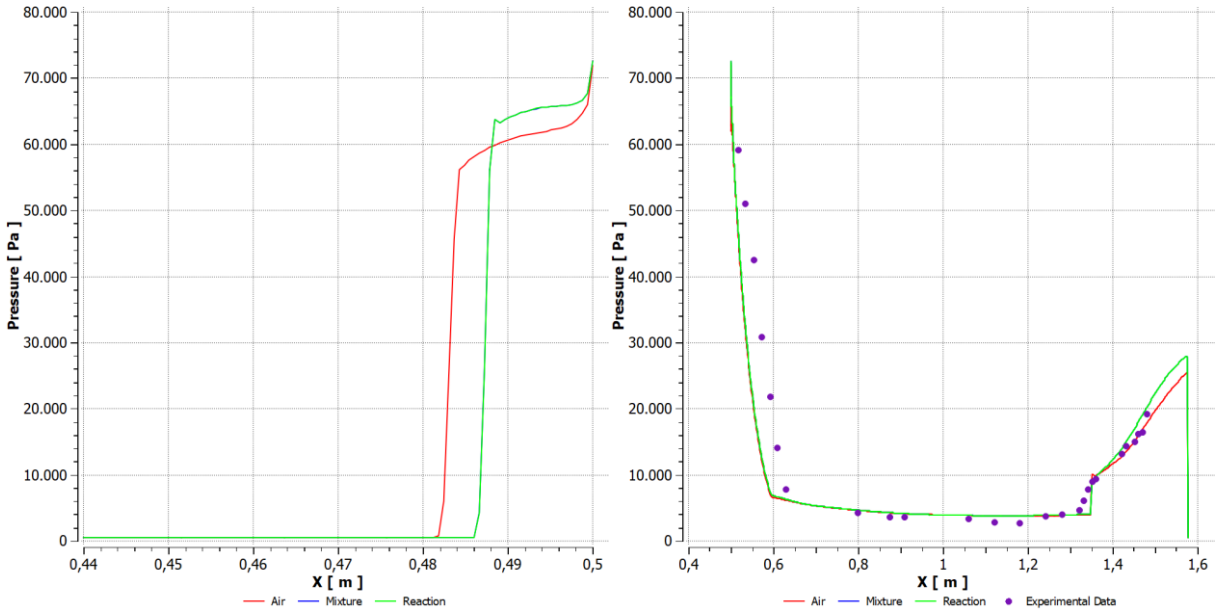

(a) (b)

Figure 13: Pressure distributions along (a) the stagnation streamline (b) along the blunt cone for Run 59

Figure 13 shows the pressure distribution along the upstream stagnation streamline in front of the leading edge in (a) and along the surface of the test body in (b) for Run 59.

By comparing three different cases in Figure 13 (a), it can be clearly seen that detached bow shock is thicker than the other two cases in which air is used as fluid. Shock wave thicknesses are expected to differ in the cases with different fluids.

In Figure 13 (b), results are given for 3 different cases by comparing with the experimental data. Some discrepancies are found in the pressure distribution on the nose of the test body as shown in the range of about 0.50-0.65 meters. As for the rest of the test body which takes the inclined surface and the flare in, good correlation is found. Also, it is confirmed that there is no reaction occurred in the reaction modeled case.

The deviation from the experimental results which is more in the nose region and less in the other regions may be caused by the effects of vibrational non-equilibrium that occur upstream of the leading edge, because these effects are not accounted by the software.

Run 63:

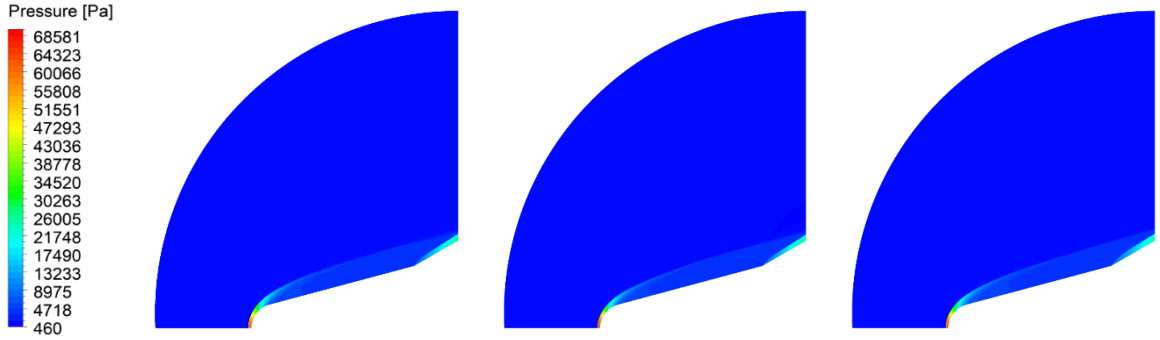

(a) (b) (c)

Figure 14: Pressure contours for Run 63 (air, mixture & reaction, respectively)

When the contours are roughly examined, similar results to Run 63 are found. So, these contours only give a general idea of pressure distributions for now. In order to observe the differences, Figures 16 (a) and (b) should be examined.

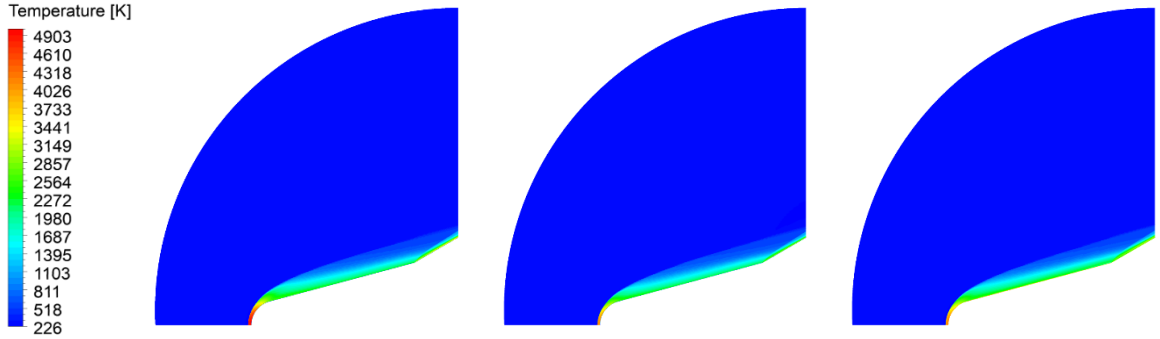

(a) (b) (c)

Figure 15: Temperature contours for Run 63 (air, mixture & reaction, respectively)

With the difference of Run 59, four different reactions modeled are expected to affect the results. It is also important to note that the boundary conditions of Run 63 are slightly different from Run 59, as given in the previous section. Also, temperatures of 4000 K and above are achieved which are required [Anderson, 2006] for the dissociation reaction of N_2. Thus, dissociation effects of N_2 are expected at the leading edge of the test body where required and higher temperatures are present.

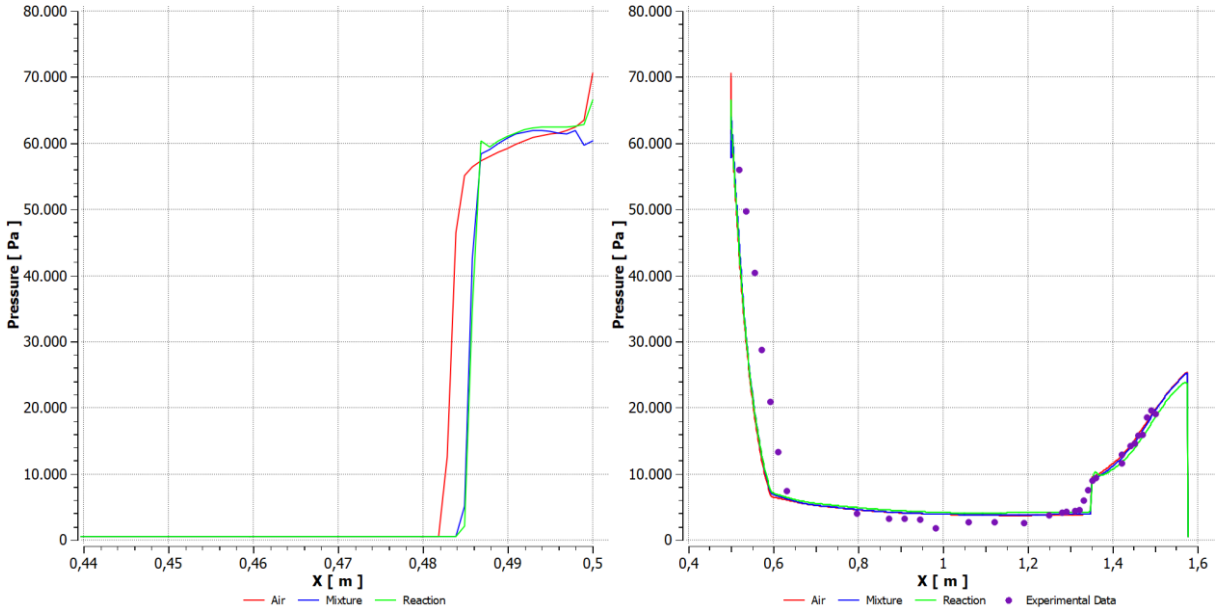

(a) (b)

Figure 16: Pressure distributions along (a) the stagnation streamline (b) along the blunt cone for Run 63

It is still predicted that the underestimation of the pressure at the leading edge is due to the vibrational non-equilibrium effects that cannot be modeled, similarly to Run 59. It is also observed that the thickness of the bow shock that appears upstream of the leading edge is shorter with chemical reactions which is a characteristic effect of chemical reactions on bow shocks. Although very small, it can be seen that there is a difference. The closest bow shock wave to the leading edge is observed in the reacted case which is an evident that taking into account for reacting gas modeling.

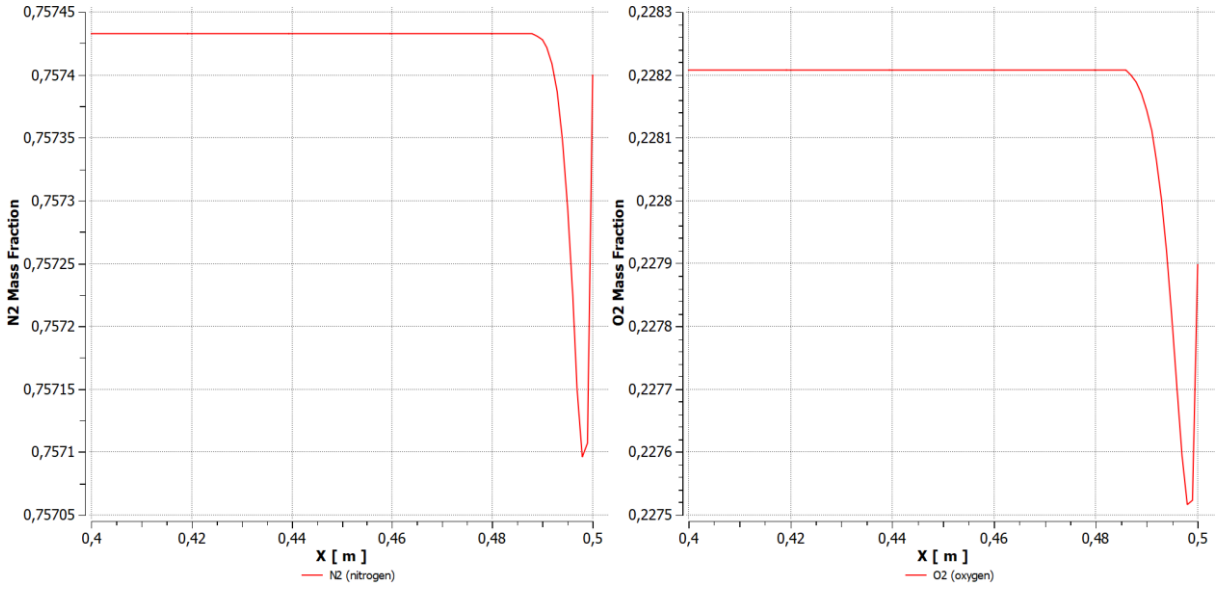

(a) (b)

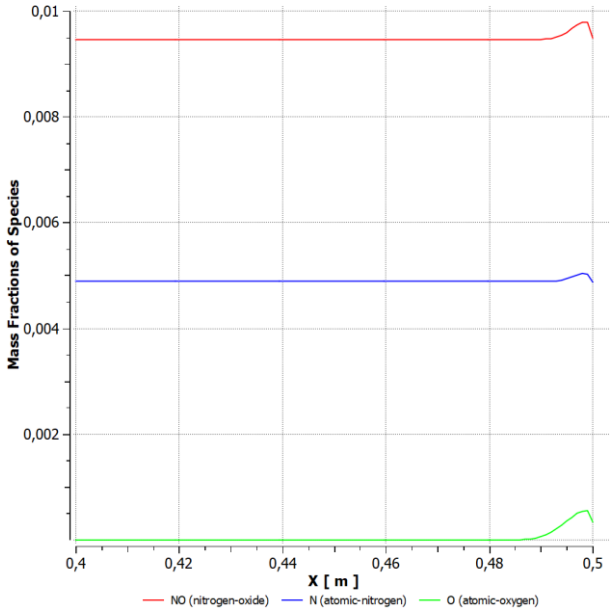

(c)

Figure 17: Mole fraction charts of the species along upstream of the leading edge for Run 63

Figures 17 (a), (b) and (c) show the mole fractions of the species are found in upstream of the leading edge for Run 63 and confirms that the expected reactions are occurred. The reason for the decreasing and increasing the mole fractions is that the reactions are reversible and defined in this way with enabling backward option.

Carbuncle Phenomenon:

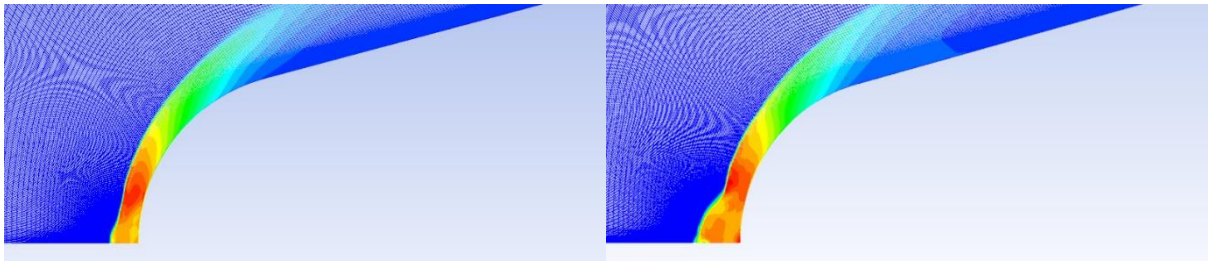

(a) (b)

Figure 18: Carbuncle phenomenon contours for Run 63

While solving the blunt cone model case, we encountered a numerical shock wave instability called carbuncle phenomenon which is not a new trend in simulating hypersonic flow [MacCormack, 2011]. By using the solution methods mentioned in the previous section to overcome this numerical problem, results unaffected by this phenomenon are obtained. It is also important to note that, neither to overcome nor to develop a solution approach for the carbuncle phenomenon are not scope of the present study.

CONCLUSION

Various validation and reaction modeling cases are performed by a commercial CFD software to verify its strengths and limitations in real gas flow fields. The first study validated with a strong detached shock expected for a sharp-cone-flare test body. The second study validated vibrational and chemical non-equilibrium effects by using species transport and reaction modeling settings of the software for a blunt cone with flare.

In respect of the sharp-cone-flare case, good correlation is found for validation with experimental data. Required boundary conditions are established for the reaction case. Some

unexpected results are occurred in this case. These results may be caused by turbulence-chemistry interaction effects which are not taken into account and/or due to the lack of vibrational non-equilibrium effects.

In respect of the blunt cone model case, good correlation is found with some discrepancies due to lack of modeling vibrational non-equilibrium between the experimental data. Pressure and temperature contours are created, and validation study is performed. It is confirmed that the dissociations are occurred with hugely increasing temperature and the mass fraction of the molecules are changing near these high temperature regions.

Improvements on the real gas simulations are observed in the results of some studies which simulates with user defined functions (UDF's) [Shoev *et al.*, 2016]. Future studies can be focus on defining UDF's to model vibrational non-equilibrium effects that can provide to use Park model much more effectively. Thus, the software can acquire the ability to model vibrational non-equilibrium effects which are most important effects that cause distortions for simulations of real gas flows. In addition, these flow fields in higher velocities can be simulated with the other Park models which are containing more reactions and chemical species.

References

Anderson Jr, J. D. (2006). *Hypersonic and high-temperature gas dynamics*. American Institute of Aeronautics and Astronautics.

Anderson, J. D. (2003) *Modern Compressible Flow: With Historical Perspective.* 3. McGraw-Hill Education (Aeronautical and Aerospace Engineering Series).

ANSYS, I. (2010). FLUENT user's guide.

Aupoix, B., & Cousteix, J. (1992). Real gas effects in two- and three-dimensional hypersonic, laminar boundary layers. Computational methods in hypersonic aerodynamics (A 93-49521 21-02). Southampton, United Kingdom/Dordrecht, Netherlands, Computational Mechanics Publications/Kluwer Academic Publishers, 1992, 293-339.

Holden, M., Bergman, R., Harvey, J., Boyd, I., Jyothish, G., Holden, M., ... & Jyothish, G. (1997, January). Experimental studies of real-gas effects over a blunted cone/flare configuration in hypervelocity airflows. In *35th Aerospace Sciences Meeting and Exhibit* (p. 855).

Kadoya, K., Matsunaga, N., & Nagashima, A. (1985). Viscosity and thermal conductivity of dry air in the gaseous phase. *Journal of physical and chemical reference data*, *14*(4), 947-970.

Kuenen, J. P., & Clark, A. L. (1917). Critical Point, Critical Phenomena and a Few Condensation Constants of Air. *Commun. Phys. Lab. Univ. Leiden*, *150*, 124.

Kussoy, M. I., & Horstman, C. C. (1989). Documentation of two-and three-dimensional hypersonic shock wave/turbulent boundary layer interaction flows.

McBride, B. J., Gordon, S., & Reno, M. A. (1993). Coefficients for calculating thermodynamic and transport properties of individual species.

MacCormack, R. (2011, January). The carbuncle cfd problem. In 49th AIAA Aerospace Sciences Meeting including the New Horizons Forum and Aerospace Exposition (p. 381).

Oliden, D. (2013). *Parametric Analysis of a Hypersonic Inlet using Computational Fluid Dynamics*. Arizona State University.

Park, C., & Lee, S. H. (1995). Validation of multitemperature nozzle flow code. Journal of thermophysics and heat transfer, 9(1), 9-16.

Savino, R., & Paterna, D. (2005). Blunted cone–flare in hypersonic flow. *Computers & fluids*, *34*(7), 859-875.

Shoev, G. V., Bondar, Y. A., Oblapenko, G. P., & Kustova, E. V. (2016). Development and testing of a numerical simulation method for thermally nonequilibrium dissociating flows in ANSYS Fluent. *Thermophysics and Aeromechanics*, *23*(2), 151-163.

Sockalingam, S., & Tabiei, A. (2016). Fluid/thermal/chemical non-equilibrium simulation of hypersonic reentry vehicles. *The International Journal of Multiphysics*, *3*(3).

Span, R., Lemmon, E. W., Jacobsen, R. T., Wagner, W., & Yokozeki, A. (2000). A reference equation of state for the thermodynamic properties of nitrogen for temperatures from 63.151 to 1000 K and pressures to 2200 MPa. *Journal of Physical and Chemical Reference Data*, *29*(6), 1361-1433.

Van der Waals, J. D. (1873). Over de Continuiteit van den Gas-en Vloeistoftoestand (Vol. 1). Sijthoff.

Wadhams, T. P., Mundy, E., MacLean, M. G., & Holden, M. S. (2008). Ground test studies of the HIFiRE-1 transition experiment part 1: experimental results. *Journal of Spacecraft and Rockets*, *45*(6), 1134-1148.

Warnatz, J., Riedel, U., & Schmidt, R. (1992). Different levels of air dissociation chemistry and its coupling with flow models. In Advances in Hypersonics (pp. 67-103). Birkhäuser, Boston, MA.